PHYSICAL REVIEW D **94,** 054507 (2016)

Short-distance charmonium correlator on the lattice with Möbius domain-wall fermion and a determination of charm quark mass

Katsumasa Nakayama,[1,2,*] Brendan Fahy,[2] and Shoji Hashimoto[2,3]
(JLQCD Collaboration)

[1]*Department of Physics, Nagoya University, Nagoya 464-8602, Japan*
[2]*KEK Theory Center, High Energy Accelerator Research Organization (KEK), Tsukuba 305-0801, Japan*
[3]*School of High Energy Accelerator Science, The Graduate University for Advanced Studies (Sokendai), Tsukuba 305-0801, Japan*

(Received 7 June 2016; published 15 September 2016)

We calculate charmonium correlators on the lattice with $2+1$ flavors of sea quarks and charm valence quarks, both described by the Möbius domain-wall fermion. Temporal moments of the correlators are calculated and matched to perturbative QCD formulas to extract the charm quark mass $m_c(\mu)$ and strong coupling constant $\alpha_s(\mu)$. Lattice data at three lattice spacings, 0.044, 0.055, and 0.080 fm, are extrapolated to the continuum limit. The correlators in the vector channel are confirmed to be consistent with the experimental data for $e^+e^- \to c\bar{c}$, while the pseudoscalar channel is used to extract $m_c(\mu)$ and $\alpha_s(\mu)$. We obtain $m_c(3\ \mathrm{GeV}) = 1.003(10)$ GeV and $\alpha_s^{\overline{\mathrm{MS}}(4)}(3\ \mathrm{GeV}) = 0.253(13)$. The dominant source of the error is the truncation of perturbative expansion at α_s^3.

DOI: 10.1103/PhysRevD.94.054507

I. INTRODUCTION

Numerical simulation of lattice QCD offers nonperturbative calculation of correlation functions on the Euclidean lattice. While one usually uses the long-distance correlators to extract the mass and matrix elements of hadrons, the same correlators at short distances also provide a rich source of information. The vector current correlator, for instance, may be used to test QCD by comparing the lattice calculation with the experimental data available for the R ratio $\sigma_{e^+e^-\to q\bar{q}}/\sigma_{e^+e^-\to\mu^+\mu^-}$. The correlator becomes mostly perturbative at high energy scales, but the nonperturbative effect is still important. Another important use of the short-distance regime is the application of perturbation theory, from which one can extract the fundamental parameters such as the strong coupling constant α_s and charm quark mass m_c.

The HPQCD and Karlsruhe collaborations used the pseudoscalar charmonium correlator to achieve a precise determination of m_c and α_s [1], which has further been improved and extended to include the determination of the bottom quark mass [2,3]. The basic idea is to use a perturbative QCD calculation performed at the order of α_s^3 to express temporal moments of the charmonium correlator calculated nonperturbatively on the lattice. Since the perturbative expansion is given as a function of α_s and m_c, one can solve the equations to determine these parameters. The precision achieved is among the best for these important fundamental parameters of QCD.

In this work, we utilize the same method to extract m_c and α_s. Our lattice data are independent of those used by the HPQCD Collaboration. We use the lattice ensembles generated with $2+1$ flavors of light sea quarks described by the Möbius domain-wall fermion formulation [4]. The valence charm quark is also treated by the same fermion formulation. Discretization effects expected for relatively large charm quark mass compared to the lattice spacing are largely removed by extrapolating to the continuum limit using the data at three lattice spacings, $a \simeq 0.080$, 0.055, and 0.044 fm. The light quark masses in the simulations are in the range corresponding to the pion masses of 230–500 MeV, which do not cover the physical value but their effect on the charmonium correlator is minor.

On the perturbative side, we use the same perturbative coefficients as those in the previous works [1–3]. We estimate the truncation error by examining the dependence on the renormalization scale μ_α to define the coupling constant $\alpha_s(\mu_\alpha)$ as well as that on μ_m that defines the running charm quark mass $m_c(\mu_m)$ appearing in the perturbative expansion.

Our results are in reasonable agreement with those of Refs. [1–3]. The estimated error is slightly larger, because of different systematic effect as well as different error estimates. We also try to validate the lattice calculation by providing a comparison to the experimental data available for the vector channel through the R ratio. It mainly serves as a test of the discretization effects, which is an important source of the systematic error for heavy quarks. We find that the continuum extrapolation is nearly flat, confirming

*katumasa@post.kek.jp

that the discretization error for charm quark is well under control in our setup.

This paper is organized as follows. In Sec. II, we review the method of Refs. [1–3] as well as the formulas to compare the temporal moments with the experimental data. Some details of our lattice calculation are given in Sec. III. Lattice results for the vector current correlator and the comparison with the experimental data are given in Sec. IV, which is followed by corresponding results for the pseudoscalar correlator in Sec. V. The issues in the matching to perturbative results and its possible uncertainties are discussed in Sec. VI, and results for charm quark mass and strong coupling constant are finally given in Sec. VII. Our conclusions are in Sec. VIII.

II. CHARMONIUM CORRELATORS AND THEIR TEMPORAL MOMENTS

A. Charmonium correlators

We calculate the pseudoscalar and vector charmonium correlators with vanishing spatial momentum

$$G^{\mathrm{PS}}(t) = a^6 \sum_{\boldsymbol{x}} (am_c)^2 \langle 0|j_5(\boldsymbol{x},t) j_5(0,0)|0\rangle, \tag{2.1}$$

$$G^{V}(t) = \frac{a^6}{3} \sum_{k=1}^{3} \sum_{\boldsymbol{x}} Z_V^2 \langle 0|j_k(\boldsymbol{x},t) j_k(0,0)|0\rangle \tag{2.2}$$

on the lattice. The currents are defined as $j_5 = i\bar{\psi}_c \gamma_5 \psi_c$ and $j_k = \bar{\psi}_c \gamma_k \psi_c$ with charm quark field ψ_c on the lattice. Given the factor a^6, both $G^{\mathrm{PS}}(t)$ are $G^V(t)$ are dimensionless. The pseudoscalar density operator j_5 is multiplied by a (bare) charm quark mass m_c such that the correlator becomes renormalization scale invariant, while a possible renormalization factor Z_V for the vector current j_k defined on the lattice is explicitly multiplied in Eq. (2.2).

We then construct the temporal moments as

$$G_n^{\mathrm{PS}} = \sum_t \left(\frac{t}{a}\right)^n G^{\mathrm{PS}}(t), \tag{2.3}$$

$$G_n^{V} = \sum_t \left(\frac{t}{a}\right)^n G^{V}(t), \tag{2.4}$$

with n an even integer equal to or larger than 4. (The correlator $\langle 0|j(x)j(0)|0\rangle$ diverges as $1/|x|^6$ in the small-separation limit, and the lower moments contain ultraviolet divergences.) On the lattice, the time coordinate t/a runs between $-T/2a+1$ and $T/2a$ with T the temporal extent of the lattice.

Since the charmonium correlators $G^{\mathrm{PS}}(t)$ and $G^V(t)$ decay exponentially at large t by the mass of the corresponding lowest energy states η_c and J/ψ, respectively, the temporal moments (2.3) and (2.4) are sensitive only to the relatively short-range correlations. For an exponential function e^{-Mt}, where M represents the mass of η_c or J/ψ, the largest contribution to the nth moment comes from the region of $t \sim n/M$. In the presence of excited state contributions, the dominant region is slightly shifted to smaller t's. Figure 1 illustrates typical examples of the integrand $(t/a)^n G^{\mathrm{PS}}(t)$ to construct the nth moments. Lattice data at $a = 0.044$ fm are taken, and data for $n = 4$, 8, and 12 are shown. The lowest moment, $n = 4$, receives a significant contribution from the small t range, $(t/a) \simeq 1$–2, where the discretization effect could be substantial. For higher moments $n = 8$ and 12, the sum is not affected much by the small t range.

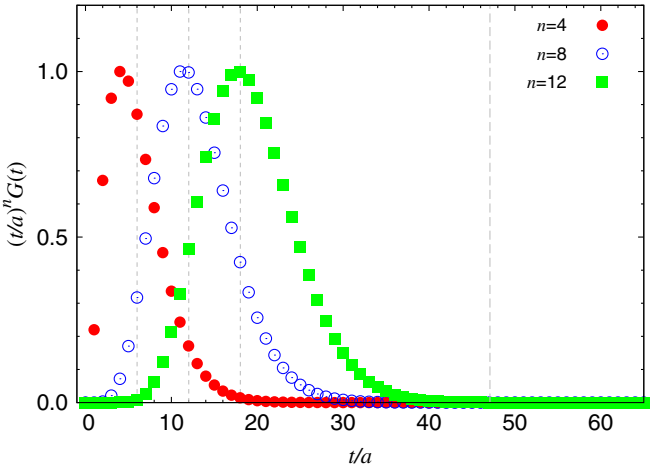

FIG. 1. $(t/a)^n G(t)$ on the lattice of size $64^3 \times 128$ at $a = 0.044$ fm. The function is normalized by its peak. The data for $n = 4$ (filled circle), 8 (open circle), and 12 (square) are shown. The long-dashed line around $t/a \sim 48$ represents the point of $\pi/(300\ \mathrm{MeV})$, which is the distance that the nonperturbative effect dominates. Three vertical dashed lines show the position of peak n/M ($n = 4$, 8 and 12) for the single exponential function e^{-Mt}. Here, $Ma = 0.6656$.

The vector correlator and its moments may be related to those in the continuum theory and to the experimental data. The vacuum polarization function $\Pi^V(q^2)$ is defined through

$$(q^\mu q^\nu - q^2 g^{\mu\nu})\Pi^V(q^2) = i \int d^4x e^{iqx} \langle 0|j^\mu(x) j^\nu(0)|0\rangle. \tag{2.5}$$

Derivatives of $\Pi^V(q^2)$ with respect to q^2,

$$g_{2k+2}^V = (2m(\mu))^{2k} \frac{12\pi^2 Q_f^2}{k!} \left(\frac{\partial}{\partial q^2}\right)^k (\Pi^V(q^2))|_{q^2=0}, \tag{2.6}$$

may be related to the experimental data for the $e^+e^- \to c\bar{c}$ process, i.e., the R ratio $R(s) \equiv \sigma_{e^+e^-\to c\bar{c}}(s)/\sigma_{e^+e^-\to\mu^+\mu^-}(s)$, as

$$\frac{12\pi^2 Q_f^2}{k!}\left(\frac{\partial}{\partial q^2}\right)^k (\Pi(q^2))|_{q^2=Q_0^2} = M_k \equiv \int_{s_0}^{\infty} ds \frac{1}{(s-Q_0^2)^{k+1}} R(s). \quad (2.7)$$

Here, Q_f stands for the electromagnetic charge of the charm quark. The lower end of the integral s_0 should be set below the J/ψ mass. The reference scale Q_0^2 is arbitrary but is often taken at $Q_0^2 = 0$. Using this notation, we may write the relation between the temporal moments on the lattice and the observable as

$$G_n^V = \frac{g_n^V}{(am(\mu))^{n-2}}. \quad (2.8)$$

A direct comparison of the lattice results with the experimental values for M_n (or their phenomenological estimates) is given in Sec. IV. The phenomenological estimates of M_n can be found in Refs. [5–8].

For the pseudoscalar density correlator

$$q^2\Pi^{\mathrm{PS}}(q^2) = i\int d^4x e^{iqx}\langle 0|j_5(x)j_5(0)|0\rangle, \quad (2.9)$$

there is no such experimental information available, while the relation between the temporal moments and the derivatives of the vacuum polarization function may be written as

$$G_n^{\mathrm{PS}} = \frac{g_n^{\mathrm{PS}}}{(am(\mu))^{n-4}} \quad (2.10)$$

with g_n^{PS} analogously defined as in Eq. (2.6).

The continuum vacuum polarization functions can be parametrized as

$$\Pi^{\mathrm{PS}}(q^2) = \frac{3}{16\pi^2}\sum_{k=-1}^{\infty} C_k^{\mathrm{PS}} z^k, \quad (2.11)$$

$$\Pi^{V}(q^2) = \frac{3}{16\pi^2}\sum_{k=-1}^{\infty} C_k^{V} z^k, \quad (2.12)$$

with $z = q^2/(2m_c(\mu))^2$. In perturbation theory, the coefficients C_k^{PS} and C_k^V are expanded in terms of $\alpha_s(\mu)/\pi$:

$$C_k = C_k^{(0)} + \frac{\alpha_s(\mu)}{\pi}(C_k^{(10)} + C_k^{(11)} l_m) + \left(\frac{\alpha_s(\mu)}{\pi}\right)^2 (C_k^{(20)} + C_k^{(21)} l_m + C_k^{(22)} l_m^2) + \left(\frac{\alpha_s(\mu)}{\pi}\right)^3 (C_k^{(30)} + C_k^{(31)} l_m + C_k^{(32)} l_m^2 + C_k^{(33)} l_m^3) + \cdots, \quad (2.13)$$

with $l_m = \log(m_c^2(\mu)/\mu^2)$. (Here, C_k and its expansion coefficients are those of either C_k^{PS} or C_k^V.) The perturbative calculation has been performed up to $O(\alpha_s^3)$ [2,5,6,8–13]. The calculation is conventionally performed in the $\overline{\mathrm{MS}}$ renormalization scheme, and the coupling constant $\alpha_s(\mu)$ and running quark mass $m_c(\mu)$ are given in that scheme at a renormalization scale μ. The relevant coefficients for $n_f = 4$ are summarized in Tables I and II for pseudoscalar and vector channels, respectively.

B. Formulas for the extraction of m_c and α_s

For the extraction of the charm quark mass and strong coupling constant, we impose the equality between the lattice and perturbative moments, following the method introduced in Refs. [1,2]. In the following, we consider the pseudoscalar channel unless otherwise stated and suppress the superscript PS.

To reduce the discretization effects, we define the reduced moment R_n using the moment $G_n^{(0)}$ evaluated at tree level using the same lattice formulation. Namely,

$$R_n = \begin{cases} \frac{G_4}{G_4^{(0)}} & \text{for } n = 4, \\ \frac{am_{\eta_c}}{2a\tilde{m}_c}\left(\frac{G_n}{G_n^{(0)}}\right)^{1/(n-4)} & \text{for } n \geq 6. \end{cases} \quad (2.14)$$

$$R_n^V = \frac{am_{J/\psi}}{2a\tilde{m}_c}\left(\frac{G_n^V}{G_n^{V(0)}}\right)^{1/(n-2)} \quad \text{for } n \geq 4. \quad (2.15)$$

TABLE I. Perturbative coefficients for the pseudoscalar correlator. The results for $n_f = 4$ are summarized from Refs. [8,9].

n	k	$C_k^{(0)}$	$C_k^{(10)}$	$C_k^{(11)}$	$C_k^{(20)}$	$C_k^{(21)}$	$C_k^{(22)}$	$C_k^{(30)}$	$C_k^{(31)}$	$C_k^{(32)}$	$C_k^{(33)}$
4	1	1.33333	3.11111	0.00000	0.115353	−6.48148	0.00000	−1.22241	2.50084	13.5031	0.00000
6	2	0.533333	2.06420	1.06667	7.23618	1.590947	−0.0444444	7.06593	−7.58522	0.550549	0.0320988
8	3	0.304762	1.21171	1.21905	5.99920	4.33726	1.16825	14.5789	7.36258	4.25232	−0.0649030
10	4	0.203275	0.712756	1.21905	4.26701	4.80644	2.38730	13.3285	14.7645	11.0345	1.45891
12	5	0.1478	0.4013	1.1821	2.9149	4.3282	3.4971		16.0798	16.6772	4.4685
14	6	0.1137	0.1944	1.1366	1.9656	3.4173	4.4992		14.1098	19.9049	8.7485
16	7	0.0909	0.0500	1.0912	1.3353	2.2995	5.4104		10.7755	20.3500	14.1272
18	8	0.0749	−0.0545	1.0484	0.9453	1.0837	6.2466		7.2863	17.9597	20.4750

TABLE II. Perturbative coefficients for the vector correlator. The results for $n_f = 4$ are summarized from Refs. [8,9,11].

n	k	$C_k^{(0)}$	$C_k^{(10)}$	$C_k^{(11)}$	$C_k^{(20)}$	$C_k^{(21)}$	$C_k^{(22)}$	$C_k^{(30)}$	$C_k^{(31)}$	$C_k^{(32)}$	$C_k^{(33)}$
4	1	1.06667	2.55473	2.13333	2.49671	3.31303	−0.0888889	−5.64043	4.06686	0.959031	0.0641975
6	2	0.457142	1.10956	1.82857	2.77702	5.14888	1.75238	−3.49373	6.72161	6.49161	−0.0973544
8	3	0.270899	0.519396	1.62540	1.63882	4.72072	3.18307	−2.83951	7.57355	13.1654	1.94521
10	4	0.1847	0.2031	1.4776	0.7956	3.6440	4.3713	−3.349	4.9487	17.4612	5.5856
12	5	0.1364	0.0106	1.3640	0.2781	2.3385	5.3990		0.9026	18.7458	10.4981
14	6	0.1061	−0.1158	1.2730	0.0070	0.9553	6.3121		−3.1990	16.9759	16.4817
16	7	0.0856	−0.2033	1.1982	−0.0860	−0.4423	7.1390		−6.5399	12.2613	23.4000
18	8	0.0709	−0.2660	1.1351	−0.0496	−1.8261	7.8984		−8.6310	4.7480	31.1546

Here, m_{η_c} ($m_{J/\psi}$) represents the mass of the η_c (J/ψ) meson calculated on the lattice, and $\tilde{m}_c$ is the charm quark pole mass at the tree level on the same lattice ensemble. For domain-wall fermions, the pole mass at tree level is given by

$$a\tilde{m}_c = am_c\left[1 - \frac{1}{6}(am_c)^2 - \frac{7}{40}(am_c)^4 - \frac{5}{112}(am_c)^6 + \frac{53}{1152}(am_c)^8 + \cdots\right] \tag{2.16}$$

as a function of the input quark mass am_c on the lattice. Details are in Appendix A. The correction term starts at $(am_c)^2$, and its size is 3.9% at $am_c = 0.4404$, which corresponds to the input charm quark mass on our coarsest lattice. This correction is expected to partly cancel the discretization effect in the calculation of am_{η_c}. Overall, in the ratios of Eq. (2.14), the discretization effects cancel between numerator and denominator at the leading order, i.e., $O(\alpha_s^0)$, and the remaining error starts at $O(\alpha_s a^2)$ for $O(a)$-improved lattice actions.

Another definition of the reduced moment $\tilde{R}_n$ is used in Ref. [3]:

$$\tilde{R}_n = \frac{a}{a\tilde{m}_c}\left(\frac{G_n}{G_n^{(0)}}\right)^{1/(n-4)} \quad \text{for } n \geq 6. \tag{2.17}$$

It does not involve the meson mass am_{η_c} and thus is free from the fitting error of the correlator using the exponential function $\exp(-(am_{\eta_c})(t/a))$. On the other hand, it contains an explicit factor of the lattice spacing a, and the error of the input for the lattice scale directly reflects in the result of m_c. The advantage of having the factor $m_{\eta_c}/\tilde{m}_c$ (or $m_{J/\psi}/\tilde{m}_c$) in Eq. (2.14) [or in Eq. (2.15)] is that the meson mass m_{η_c} (or $m_{J/\psi}$) effectively plays the role of the input scale to determine m_c. With $\tilde{R}_n$, the error in setting the lattice spacing, which is about 1.7% in our case, directly appears in the final result for m_c. We analyzed the data for both R_n and $\tilde{R}_n$, and it turned out that R_n gives more precise determination. Only the results with R_n are presented in this paper.

On the continuum side, one defines the reduced moment r_n from the derivatives of $q^2\Pi(q^2)$ with respect to q^2,

$$g_{2k} \equiv \frac{12\pi^2 Q_f^2}{k!}\left(\frac{\partial}{\partial z}\right)^k (z\Pi(q^2))|_{q^2=0} = \frac{12\pi^2 Q_f^2}{(k-1)!}\left(\frac{\partial}{\partial z}\right)^{k-1} (\Pi(q^2))|_{q^2=0}, \tag{2.18}$$

as

$$r_n = \begin{cases} g_4/g_4^{(0)} = C_1/C_1^{(0)} & \text{for } n = 4, \\ (g_n/g_n^{(0)})^{1/(n-4)} = (C_{n/2-1}/C_{n/2-1}^{(0)})^{1/(n-4)} & \text{for } n \geq 6. \end{cases} \tag{2.19}$$

$$r_n^V = (g_n^V/g_n^{V(0)})^{1/(n-2)} = (C_{n/2-1}/C_{n/2-1}^{(0)})^{1/(n-2)} \quad \text{for } n \geq 4. \tag{2.20}$$

The tree-level moment $g_n^{(0)}$ can be explicitly written as [14]

$$g_{2n+2}^{(0)} = 12\pi^2 Q_f^2 \frac{3}{8\pi^2}\frac{2^n(n-1)!}{(2n+1)!!}, \tag{2.21}$$

and $g_{2k+2}^{V(0)}$ can be written as

$$g_{2n+2}^{V(0)} = 12\pi^2 Q_f^2 \frac{1}{4\pi^2}\frac{2^n(n+1)(n-1)!}{(2n+3)!!}. \tag{2.22}$$

Then, the equality (2.10) may be rewritten as

$$R_n = \frac{m_{\eta_c}^{\text{exp}}}{2m_c(\mu)} r_n(\alpha_s(\mu), m_c(\mu)). \tag{2.23}$$

Here, r_n is a function of $\alpha_s(\mu)$ and $m_c(\mu)$, and the equation is understood as a condition to be satisfied by the parameters $\alpha_s(\mu)$ and $m_c(\mu)$ when a numerical value for R_n is nonperturbatively calculated on the lattice. We can also use a ratio of the reduced moments,

TABLE III. Lattice ensembles used in this study.

β	a^{-1} (GeV)	$L^3 \times T(\times L_5)$	$N_{\rm src}$	#meas	am_{ud}	am_s	m_π (MeV)	$m_\pi L$	id
4.17	2.453(4)	$32^3 \times 64(\times 12)$	8	800	0.0035	0.040	230(1)	3.0	*C-ud2-sa*
					0.007	0.030	310(1)	4.0	*C-ud3-sb*
					0.007	0.040	309(1)	4.0	*C-ud3-sa*
					0.012	0.030	397(1)	5.2	*C-ud4-sb*
					0.012	0.040	399(1)	5.2	*C-ud4-sa*
					0.019	0.030	498(1)	6.5	*C-ud5-sb*
					0.019	0.040	499(1)	6.5	*C-ud5-sa*
		$48^3 \times 96(\times 12)$	8	800	0.0035	0.040	226(1)	4.4	*C-ud2-sa*-L
4.35	3.610(9)	$48^3 \times 96(\times 8)$	12	600	0.0042	0.0180	296(1)	3.9	*M-ud3-sb*
					0.0042	0.0250	300(1)	3.9	*M-ud3-sa*
					0.0080	0.0180	407(1)	5.4	*M-ud4-sb*
					0.0080	0.0250	408(1)	5.4	*M-ud4-sa*
					0.0120	0.0180	499(1)	6.6	*M-ud5-sb*
					0.0120	0.0250	501(1)	6.6	*M-ud5-sa*
4.47	4.496(9)	$64^3 \times 128(\times 8)$	8	400	0.0030	0.015	284(1)	4.0	*F-ud3-sa*

$$\frac{R_n}{R_{n+2}} = \frac{r_n(\alpha_s(\mu), m_c(\mu))}{r_{n+2}(\alpha_s(\mu), m_c(\mu))}, \tag{2.24}$$

which may play a complementary role to Eq. (2.23), since the truncation error of its perturbative expansion is different from that of individual r_n.

In QCD, the perturbation theory is reliable only in the relatively short-distance regime compared to the hadronic scale $1/\Lambda_{\rm QCD}$. To avoid the nonperturbative regime, n has to be small to satisfy a condition $n/M \ll \pi/\Lambda_{\rm QCD}$, which implies an upper limit for n, i.e., $n \ll \pi M/\Lambda_{\rm QCD}$. For the charmonium of $m \simeq 3$ GeV, this means that n has to be of order of 10 or smaller. As shown in Sec. VI B, the leading nonperturbative effect in the operator product expansion appears as a contribution of the gluon condensate. Its coefficient $a_{n/2}$ in Eq. (6.4) rapidly grows for larger n.

Combined with the lower limit for n to avoid the large discretization effect, as discussed earlier in this section, there is a limited window of n for this method to be useful. In our analyses, we chose $n = 6$, 8, and 10. There is a practical limitation for $n \geq 12$; i.e., the $O(\alpha_s^3)$ coefficients in the perturbative expansion of r_n are not available.

III. LATTICE DETAILS

We have performed a set of lattice QCD simulations with $2 + 1$ flavors of dynamical quarks. The gauge action is that of tree-level Symanzik improved, and the fermion formulation is the Möbius domain-wall fermions [4]. The gauge links are smeared by applying the stout smearing [15] three times. With this choice, the residual mass, which quantifies the violation of the Ginsparg-Wilson relation, is under good control; i.e., the residual mass is of $O(1\,\text{MeV})$ on our coarsest lattice and much smaller on finer lattices. The effect of such a small violation can be neglected for the charmonium correlators. Light sea quark masses are extrapolated to the physical value such that the physical pion and kaon masses are reproduced. Since the sea quark mass dependence of R_n is minor, this is not a major source of uncertainty.

There are 15 ensembles of different lattice spacings and quark masses as listed in Table III. Lattice spacings are $a = 0.080$, 0.055, and 0.044 fm. The spatial size of these lattices is $L/a = 32$, 48, and 64, respectively, to keep the physical lattice size L approximately constant, ~2.6–2.8 fm. The temporal size T/a is always twice longer than L/a. Each ensemble consists of 10,000 molecular dynamics trajectories, out of which we chose 50–100 gauge configurations equally separated and calculated the charmonium correlators 8 or 12 times starting from different time slices on each configuration with a Z_2 noise. The number of measurement "#meas" is thus 400–800 depending on the ensemble as listed in the table.

The Z_2 noise is introduced to improve the statistical signal. Namely, the Z_2 (± 1) noise is scattered over a time slice as a source to calculate the charm quark propagator; only the local Z_2-invariant contribution survives after averaging over the noise so that the desired contraction of charm and anticharm propagators survives and other gauge noninvariant contributions vanish. In spite of the noise introduced, the signal is improved by averaging over the source points.

Each ensemble has an "id" name, which distinguishes coarse (C), medium (M), and fine (F) lattices, as well as the mass of *ud* and *s* quark masses. In the main ensembles (C and M), two values of strange quark mass are chosen to sandwich the physical value from above (a) or from below (b). On the coarse lattice at the lightest *ud* quark mass, there is an ensemble of larger volume of size $48^3 \times 96$, which is indicated by "-L." The difference between *C-ud2-sa* and *C-ud2-sa*-L is used to estimate the possible finite-volume effect, as they have the smallest *ud* quark mass and the

effect of the finite spatial volume is expected to be most significant in our ensembles.

The lattice spacing is set through the Wilson-flow scale t_0 [16]. For its physical value, we input $t_0^{1/2} = 0.1465(21)(13)$ fm [17]. The resulting values of a^{-1} are listed in Table III. The table lists the central values and the statistical error in our measurement of t_0. The error in this input value is to be added for each value of a^{-1}.

Some details of the ensemble generation are available in Refs. [18,19]. The same gauge ensembles have so far been used for a calculation of the η' meson mass [20], an analysis of short-distance current correlator [21], and a calculation of heavy-light meson decay constants [22]. The numerical calculations are performed using the IroIro++ code set for lattice QCD [23].

For the vector current, we multiply the renormalization constant Z_V obtained from the analysis of the short-distance current correlator of light quarks [24]. The numerical values are 0.9553(92) at $\beta = 4.17$, 0.9636(58) at $\beta = 4.35$, and 0.9699(47) at $\beta = 4.47$, where errors include statistical and systematic ones added in quadrature.

On each ensemble, we calculate the charmonium correlator at a bare charm quark mass 0.4404, 0.2723, or 0.2105 at $\beta = 4.17$, 4.35, or 4.47, respectively. They are slightly mistuned to the physical charm quark mass, which we set by the spin-averaged mass of the 1S charmonium states $(m_{\eta_c} + 3m_{J/\psi})/4$. We correct this minor shift by using the supplemental data set taken at three values of bare charm quark mass sandwiching the physical value. The supplemental data are obtained with a local source and are therefore less precise, but are only used for a small interpolation of the main data to the physical charm quark mass.

In the calculation of the charmonium correlator, we do not take account of the contribution of disconnected quark-loop diagrams, which may exist in the nature for the flavor-singlet operators like $j_5 = \bar{\psi}_c \gamma_5 \psi_c$. For the correspondence between the lattice and perturbative calculations, this does not cause any problem because one can omit the corresponding diagrams also in perturbation theory. For the input to tune the charm quark mass on the lattice, this could lead to some bias, as the physical input parameter, a mass of η_c or J/ψ, includes such an effect. Furthermore, the electromagnetic correction which is neglected in our lattice calculation could also be a source of systematic error. These sources of uncertainties are discussed in some detail in Sec. VII.

IV. TEMPORAL MOMENTS OF VECTOR CURRENT CORRELATOR

As described in Sec. II, the temporal moments of the charmonium vector-current correlator can be compared with the experimental value.

Analogous to the reduced moments defined for the pseudoscalar channel (2.14), we define the reduced moments R_n^V for the vector moments (2.14). We can then write the correspondence between the lattice and continuum as

$$R_{2k+2}^V = m_{J/\psi} \left(\frac{M_k}{g_{2k+2}^{V(0)}} \right)^{\frac{1}{2k}}, \tag{4.1}$$

which is obtained from Eq. (2.8).

Numerical results for $Z_V^{\frac{2}{n-2}} R_n^V$ are summarized in Table IV for $n(=2k+2) = 6$, 8, 10, and 12. For each ensemble, the results are interpolated to the physical charm quark mass; the statistical error is propagated by the bootstrap method.

The results are linearly extrapolated to the physical light quark mass and plotted as a function of a^2 in Fig. 2. The lattice results are nearly constant in a^2, and the continuum extrapolation as discussed below is also shown.

We extrapolate R_n^V assuming the form

$$R_n^V = R_n^V(0)(1 + c_1 (a m_c)^2) \times \left(1 + f_1 \frac{m_u + m_d + m_s}{m_c} \right), \tag{4.2}$$

with free parameters $R_n^V(0)$, c_1, and f_1. The error of $O(a^2)$ is eliminated by an extrapolation with this form, while the effect of $O(a^4)$ still needs to be estimated. We attempt two continuum extrapolations assuming a linear dependence on a^2 with and without the point of the coarsest lattice. The three-point fit yields a $\chi^2/\mathrm{dof} = 0.17$ (0.40) for $n = 6$ (8). The value of χ^2/dof is slightly underestimated since the correlated systematic error for Z_V among different β values is not taken into account. We take the mean value of these two extrapolations as a central value and estimate the

TABLE IV. Reduced moment $Z_V^{\frac{2}{n-2}} R_n^V$ for each ensemble.

	$Z_V^{\frac{2}{n-2}} R_6^V$	$Z_V^{\frac{2}{n-2}} R_8^V$	$Z_V^{\frac{2}{n-2}} R_{10}^V$	$Z_V^{\frac{2}{n-2}} R_{12}^V$
C-ud2-sa	1.3563(5)	1.3101(5)	1.2722(5)	1.2429(5)
C-ud3-sb	1.3562(5)	1.3101(5)	1.2721(5)	1.2428(5)
C-ud3-sa	1.3563(5)	1.3102(5)	1.2722(5)	1.2430(5)
C-ud4-sb	1.3564(5)	1.3103(5)	1.2723(5)	1.2430(5)
C-ud4-sa	1.3576(5)	1.3112(5)	1.2731(5)	1.2437(5)
C-ud5-sb	1.3589(5)	1.3125(5)	1.2742(5)	1.2448(5)
C-ud5-sa	1.3594(5)	1.3130(5)	1.2747(5)	1.2452(5)
C-ud2-sa-L	1.3559(5)	1.3099(4)	1.2721(4)	1.2432(4)
M-ud3-sb	1.3461(7)	1.2919(6)	1.2553(6)	1.2285(6)
M-ud3-sa	1.3475(6)	1.2932(6)	1.2564(6)	1.2296(5)
M-ud4-sb	1.3483(7)	1.2939(6)	1.2571(6)	1.2302(6)
M-ud4-sa	1.3489(6)	1.2944(6)	1.2575(6)	1.2306(6)
M-ud5-sb	1.3499(7)	1.2953(6)	1.2583(6)	1.2312(6)
M-ud5-sa	1.3511(6)	1.2964(6)	1.2594(6)	1.2323(6)
F-ud3-sa	1.3435(7)	1.2892(6)	1.2536(6)	1.2275(6)

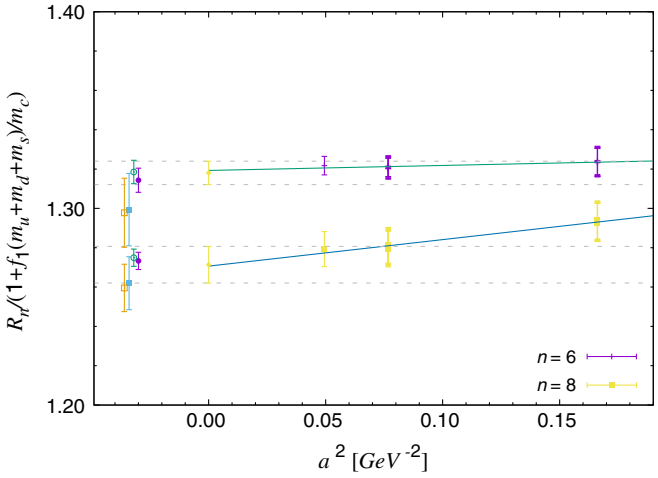

FIG. 2. Continuum extrapolation of the reduced moments for the vector current R_n^V [$n = 6$ (pluses) and 8 (squares)]. Data are plotted after correcting for the finite light quark mass effects by multiplying $1/(1 + f_1(m_u + m_d + m_s)/m_c)$. Lattice data are corrected for the missing charm quark loop effect, estimated by perturbation theory, $r_n^V(n_f = 4)/r_n^V(n_f = 3)$. The error of the individual lattice data includes that from the renormalization factor Z_V, which is the dominant source of error. The points at $a^2 = 0$ are our estimate of the continuum limit based on two methods of continuum extrapolation. Its error includes that due to the input for a^{-1} as well. Phenomenological estimates of corresponding quantities are plotted on the left: Dehnadi *et al.* [25] (filled circle), Kuhn *et al.* [7] (open circle), Kuhn *et al.* [26] (filled square), and Hoang *et al.* [27] (open square).

remaining discretization error using the deviation from the mean value.

The quark mass dependence of nonperturbative origin, which is assumed to be linear in $m_u + m_d + m_s$, turned out to be tiny ($f_1 \sim 0$), and we do not consider its higher-order effects.

Since the lattice calculation is performed with three light flavors ($n_f = 3$), we estimate the effect of the charm quark loop by perturbative theory. Namely, we correct the lattice result of $n_f = 3$ to that of $n_f = 4$, by multiplying $r_n^V(n_f = 4)/r_n^V(n_f = 3)$. The perturbative coefficients are calculated to $O(\alpha_s^2)$ [9] and partly to $O(\alpha_s^3)$ [8]. We set the number of heavy flavors $n_h = 1$ (or 0) for $n_f = 4$ (or 3) to calculate the ratio $r_n^V(n_f = 4)/r_n^V(n_f = 3)$. We also take account of the small difference of $\alpha_s^{n_f=4}(\mu)$ and $\alpha_s^{n_f=3}(\mu)$ as well as that of $m_c(\mu)$. The correction is numerically small; i.e., the factor is 0.9992(26), 1.0026(68), and 1.0156(342) for $n = 6$, 8, and 10, respectively.

Table V summarizes the results for $R_n^V(0)$. The perturbative error is estimated by taking a range of the scale $\mu = 2$–4 GeV. The large error for $n = 10$ is due to the lack of the $O(\alpha_s^3)$ formula. The results in the continuum limit are compared with the phenomenological estimates [7,25–28]. The agreement of the lattice data and the phenomenological estimates is remarkable. In particular, our data are consistent with the updated estimates with reduced error of Refs. [7,25], and the size of total error is comparable.

V. TEMPORAL MOMENTS OF PSEUDOSCALAR CURRENT CORRELATOR

The reduced moments R_n ($n = 6$, 8, 10, and 12) for the pseudoscalar channel obtained at each ensemble are listed in Table VI, and their ratios R_n/R_{n+2} are in Table VII.

By comparing the data at two different volumes, which are available for the coarse lattice with the lightest sea quarks ($\beta = 4.17$, $am_{ud} = 0.0035$), we observe that the results on the larger volume $48^3 \times 96$ (*C-ud2-sa*-L) are lower than those on $32^3 \times 64$ (*C-ud2-sa*) by about two standard deviations for R_4 and R_6. For R_8, R_{10}, and R_{12}, on the other hand, the data at different volumes coincide within the statistical error. We estimate the systematic error due to the finite-volume effect by taking these differences and applying them for all the other ensembles assuming similar values for each. This should give a conservative estimate because the finite-volume effect is expected to be significantly less for heavier sea quarks. We note that the value of $m_\pi L$ is small ($\sim$3.0) only for this ensemble (*C-ud2-sa*); others satisfy $m_\pi L > 3.9$. As listed in the table of systematic errors in final results (Table IX), the estimated error from this source is an order of magnitude smaller than other

TABLE V. Reduced moments $R_n^V(0)$ extrapolated to the continuum limit at physical light quark masses. The errors in "This work" are from statistical, discretization, finite-volume, and the input values of $t_0^{1/2}$, respectively. The numbers for $n_f = 3$ are the lattice data with $2 + 1$ flavors of dynamical quarks, while those for $n_f = 4$ are after the correction by $r_n(n_f = 4)/r_n(n_f = 3)$. The last error for "$n_f = 4$" is from this perturbative correction factor. Phenomenological estimates from Refs. [7,25–27] are shown with the estimated error in these references.

	This work		Phenomenological estimates			
	$n_f = 3$	$n_f = 4$	[25]	[7]	[26]	[27]
$R_6^V(0)$	1.3191(33)(12)(4)(34)	1.3181(33)(13)(4)(33)(34)	1.3143(61)	1.3185(59)	1.2994(184)	1.2978(176)
$R_8^V(0)$	1.2680(22)(7)(2)(28)	1.2714(22)(8)(2)(28)(86)	1.2732(44)	1.2749(44)	1.2620(135)	1.2596(120)
$R_{10}^V(0)$	1.2365(16)(13)(0)(22)	1.2558(16)(13)(0)(22)(423)	1.2439(35)	1.2447(34)	1.2352(104)	1.2330(91)

TABLE VI. Reduced moment R_n in each ensemble. The errors shown are statistical.

	R_6	R_8	R_{10}	R_{12}
C-ud2-sa	1.4689(6)	1.3681(5)	1.3087(4)	1.2679(4)
C-ud3-sb	1.4696(5)	1.3686(5)	1.3090(4)	1.2682(4)
C-ud3-sa	1.4692(5)	1.3683(5)	1.3089(4)	1.2681(4)
C-ud4-sb	1.4696(6)	1.3687(5)	1.3091(4)	1.2683(4)
C-ud4-sa	1.4706(5)	1.3693(5)	1.3097(4)	1.2687(4)
C-ud5-sb	1.4720(5)	1.3705(5)	1.3107(4)	1.2696(4)
C-ud5-sa	1.4722(6)	1.3708(5)	1.3109(4)	1.2699(4)
C-ud2-sa-L	1.4693(5)	1.3684(4)	1.3091(4)	1.2685(4)
M-ud3-sb	1.4869(6)	1.3598(5)	1.2977(5)	1.2582(4)
M-ud3-sa	1.4882(6)	1.3609(5)	1.2986(5)	1.2590(4)
M-ud4-sb	1.4888(7)	1.3611(6)	1.2987(5)	1.2590(5)
M-ud4-sa	1.4896(6)	1.3618(5)	1.2994(5)	1.2596(4)
M-ud5-sb	1.4899(7)	1.3621(5)	1.2996(5)	1.2598(5)
M-ud5-sa	1.4912(6)	1.3631(5)	1.3005(4)	1.2605(4)
F-ud3-sa	1.4961(6)	1.3616(5)	1.2987(5)	1.2590(4)

sources, and any combined error of the finite-volume effect with other sources is negligible.

We interpolate R_n in m_c to the physical point by tuning until the spin-averaged mass $(m_{\eta_c} + 3m_{J/\psi})/4$ reproduces the experimental value, 3.0687 GeV. Figure 3 shows an extrapolation of below. the spin-averaged mass to the physical pion mass. A fit is done assuming that the slope in m_π^2 is independent on β, which seems reasonable as the plot shows. The χ^2/dof of this fit is 1.9.

Our lattice results extrapolated to the physical pion mass are slightly lower than the experimental data by about 0.1%–0.3% depending on β because of a slight mistuning of the input m_c. We correct for them by using the supplemental data taken at three different m_c's for each β as discussed.

TABLE VII. Ratios of the reduced moment R_n/R_{n+2} for each ensemble. The errors shown are the measured statistical uncertainty.

	R_6/R_8	R_8/R_{10}	R_{10}/R_{12}
C-ud2-sa	1.07365(8)	1.04540(3)	1.03216(2)
C-ud3-sb	1.07381(7)	1.04548(3)	1.03220(2)
C-ud3-sa	1.07368(7)	1.04542(3)	1.03217(2)
C-ud4-sb	1.07377(7)	1.04547(3)	1.03221(2)
C-ud4-sa	1.07396(7)	1.04555(3)	1.03226(2)
C-ud5-sb	1.07406(7)	1.04563(3)	1.03234(2)
C-ud5-sa	1.07400(8)	1.04563(3)	1.03235(2)
C-ud2-sa-L	1.07369(5)	1.04529(2)	1.03204(1)
M-ud3-sb	1.09346(11)	1.04783(5)	1.03144(3)
M-ud3-sa	1.09360(9)	1.04792(4)	1.03151(2)
M-ud4-sb	1.09380(12)	1.04801(5)	1.03157(3)
M-ud4-sa	1.09384(12)	1.04802(5)	1.03158(3)
M-ud5-sb	1.09388(12)	1.04808(5)	1.03162(3)
M-ud5-sa	1.09401(9)	1.04814(4)	1.03167(2)
F-ud3-sa	1.09882(10)	1.04839(4)	1.03150(3)

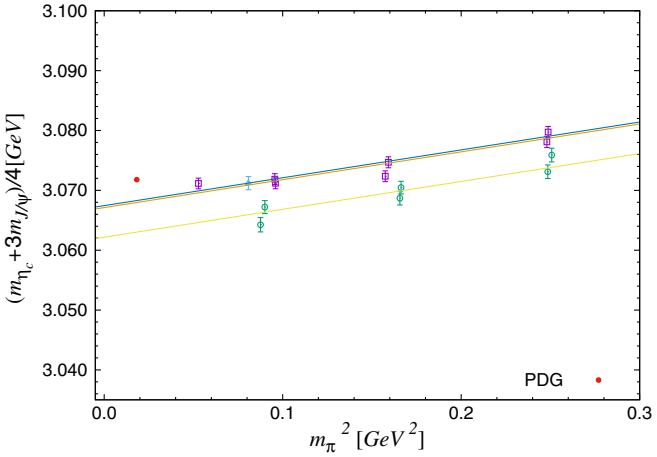

FIG. 3. Spin-averaged mass $(m_{\eta_c} + 3m_{J/\psi})/4$ as a function of m_π^2. The experimental value, 3.072 GeV, is shown by a filled circle. Data at $\beta = 4.17$ (square), $\beta = 4.35$ (circle), and $\beta = 4.47$ (triangle) are plotted. At each β, the extrapolation to the physical pion mass slightly misses the experimental value since the input m_c is not exactly tuned. This tiny difference is corrected when we analyze the temporal moments.

Figure 4 is an example of the m_c dependence of R_6 obtained at $\beta = 4.47$. Our main data point (filled square) is slightly off the target physical value of the physical $(m_{\eta_c} + 3m_{J/\psi})/4$ shown by a dashed line. We correct the data using a slope obtained from the supplemental data at three values of m_c shown in Fig. 4. The supplemental data have significantly larger statistical error but are sufficiently precise to determine the slope needed for the correction. (The fit to obtain the slope is uncorrelated. The effect of ignoring the correlation among three data points should

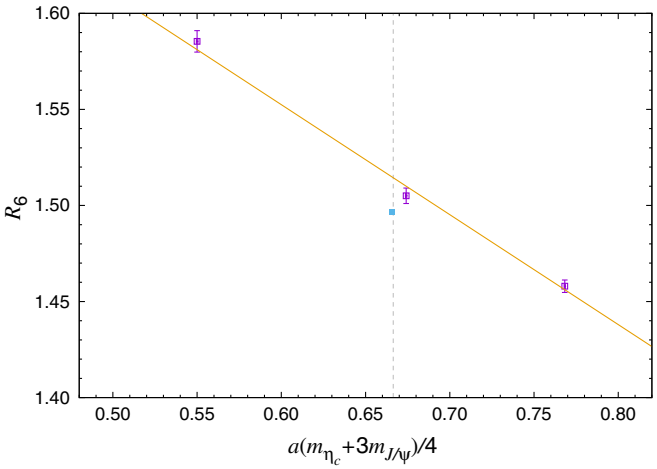

FIG. 4. R_6 as a function of the spin-averaged mass $a(m_{\eta_c} + 3m_{J/\psi})/4$ from different m_c. Data at $\beta = 4.47$ are shown. The dashed line represents the physical spin-averaged mass. Three data points shown by open square are from the supplemental data set obtained without using the Z_2 noise source. The filled square is our main data point calculated with the Z_2 noise source.

have little impact on the final result, since the correction itself is very small.) The correction factor on this ensemble is tiny, i.e., ∼0.03%.

When we interpolate to the physical point of m_c, we need to incorporate the uncertainty of the lattice spacing originating from the input value of $t_0^{1/2}$. This error is propagated to the following analysis by repeating the same analysis with the lattice spacing a set to the upper and lower limits of its uncertainty.

We extrapolate R_n to the continuum limit assuming the form similar to (4.2):

$$R_n = R_n(0)(1 + c_1(am_c)^2) \times \left(1 + f_1 \frac{m_u + m_d + m_s}{m_c}\right). \tag{5.1}$$

This continuum extrapolation is shown in Fig. 5.

The remaining discretization error is estimated as in the vector channel by taking the difference between the extrapolations with two and three data points. The lattice data at different values of a and sea quark masses are statistically independent. We use the standard χ^2 fitting; the value of χ^2/dof is 2.1, 4.1, 5.1, 4.6, and 3.9 for R_6, R_8, R_{10}, R_{12}, and R_{14}, respectively.

Table VIII summarizes the results for $R_n(0)$. The systematic error due to the finite volume is estimated as described above.

Again, we correct the lattice result of $n_f = 3$ to that of $n_f = 4$, by multiplying by $r_n(n_f = 4)/r_n(n_f = 3)$. This numerical factor is 1.0031, 1.0014, and 1.0026 for $n = 6$, 8, and 10, respectively. Table VIII lists the data before and after this correction.

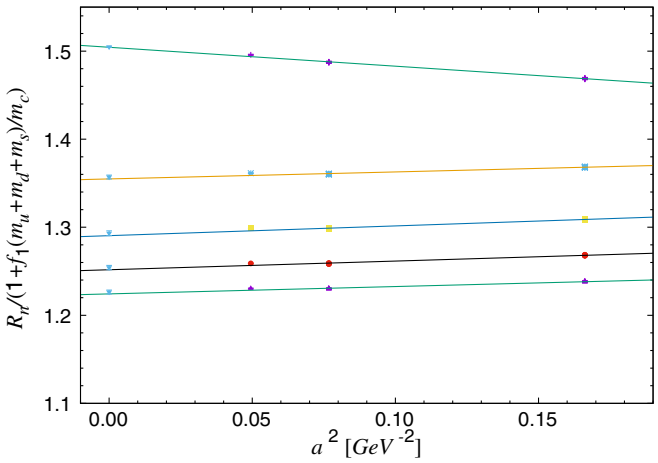

FIG. 5. Continuum extrapolation of $R_n(a)$. Data points correspond to R_6, R_8, R_{10}, R_{12}, and R_{14} from top to bottom. The continuum extrapolation assuming the form (5.1) is shown by lines. The points at $a = 0$ represent our estimate obtained from a mean of the extrapolated values with and without the coarsest lattice data.

TABLE VIII. Reduced moments R_n and their ratios extrapolated to the continuum limit at physical light quark masses. The numbers for $n_f = 3$ show our original calculation with $n_f = 2 + 1$ on the lattice, and those for $n_f = 4$ are after the correction using a factor $r_n(n_f = 4)/r_n(n_f = 3)$ for R_n or $(r_n(n_f = 4)/r_n(n_f = 3))/(r_{n+2}(n_f = 4)/r_{n+2}(n_f = 3))$ for R_n/R_{n+2}. The four errors on each value in the table are from the measured statistical variance, discretization effects, finite-volume effects, and the uncertainty from the input value of $t_0^{1/2}$, respectively.

	$n_f = 3$	$n_f = 4$
$R_6(0)$	1.5048(5)(5)(4)(66)	1.5094(5)(5)(4)(66)
$R_8(0)$	1.3570(4)(22)(3)(39)	1.3589(4)(22)(3)(39)
$R_{10}(0)$	1.2931(4)(27)(5)(27)	1.2965(4)(27)(5)(27)
$R_6(0)/R_8(0)$	1.1089(1)(13)(0)(17)	1.1108(1)(13)(0)(17)
$R_8(0)/R_{10}(0)$	1.0494(0)(5)(1)(8)	1.0481(0)(5)(1)(8)

VI. SYSTEMATIC ERRORS ON THE CONTINUUM SIDE

As summarized in Sec. II, one may use Eqs. (2.23) and (2.24) to extract $\alpha_s(\mu)$ and $m_c(\mu)$ with the lattice inputs for R_n obtained in the previous section. Several sources of systematic errors mainly on the perturbative side are discussed in this section.

A. Truncation of perturbative series

Perturbative coefficients for r_n are available up to $O(\alpha_s^3)$ as listed in Table I, and the remaining error is $O(\alpha_s^4)$. Since the left-hand side of Eq. (2.23) is independent of the renormalization scale μ, we estimate the truncation error from the residual μ dependence of the combination $r_n(\alpha_s(\mu), m_c(\mu))/m_c(\mu)$ on the right-hand side. We take $\mu = 3$ GeV for a central value and consider the variation in the range of ± 1 GeV for the estimate of the truncation error. Figure 6 shows an example for $n = 8$. The μ

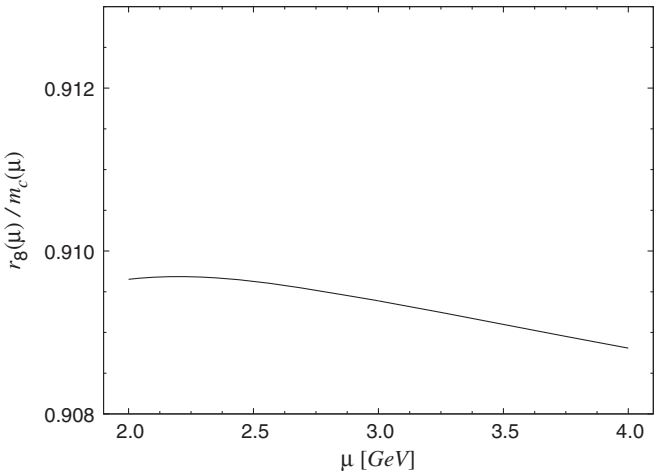

FIG. 6. Residual scale dependence of the ratio $r_n(\mu)/m_c(\mu)$. The case for $n = 8$ is plotted as a typical example.

dependence of $r_n(\alpha_s(\mu), m_c(\mu))$ is almost canceled by the dependence of $m_c(\mu)$, and the remnant μ dependence is tiny but nonzero, which we take as the truncation error.

We generalize this argument by taking the scale to define $\alpha_s(\mu)$ and $m_c(\mu)$ differently. Namely, we reorganize the perturbative series in terms of $\alpha_s(\mu_\alpha)$ and $m_c(\mu_m)$ with $\mu_\alpha \neq \mu_m$ [25,28]. This can be done by inserting an expansion of $\alpha_s(\mu = \mu_m)$ in terms of $\alpha_s(\mu_\alpha)$ into the formula of $r_n(\alpha_s(\mu), m_c(\mu))$ and rearranging the perturbative series. The terms of $O(\alpha_s^4(\mu_\alpha))$ are then truncated.

After this extension, we estimate the truncation error by taking a variation in the range $\mu_\alpha = \mu_m \pm 1$ GeV with $2\ \text{GeV} \leq \min\{\mu_\alpha, \mu_m\}$ and $\max\{\mu_\alpha, \mu_m\} \leq 4\text{GeV}$. This provides a more conservative estimate of the truncation error than simply taking $2\ \text{GeV} \leq \mu_\alpha = \mu_m \leq 4$ GeV. Because of this choice, our estimate for the truncation error is larger than those in the previous works.

B. Nonperturbative corrections

The perturbative expansion is supplemented by nonperturbative power corrections in the operator product expansion. Such power corrections should be carefully examined before applying the perturbative expansion for the current correlators.

At the lowest nontrivial order, which is of the order of $1/m_c^4$, the gluon condensate $\langle(\alpha_s/\pi)G_{\mu\nu}^2\rangle$ appears [29]. At the two-loop order, that is written as

$$\frac{\partial}{\partial q^2}(z\Pi(q^2)^{GG}) = \frac{\partial}{\partial q^2}\left(\frac{\langle(\alpha_s/\pi)G_{\mu\nu}^2\rangle}{(2m_{\rm OS})^4}\sum_\ell\left(a_\ell + \frac{\alpha_s}{\pi}c_\ell\right)z^\ell\right), \tag{6.1}$$

where $m_{\rm OS}$ is an on-shell heavy quark mass and a_ℓ and c_ℓ are numerical coefficients. The lowest-order coefficients a_ℓ for the pseudoscalar (PS) and vector (V) correlators are

$$a_\ell^{\rm PS} = -\frac{\ell-4}{12}\frac{(2)_\ell}{(3/2)_\ell}, \quad a_\ell^V = -\frac{2\ell-2}{15}\frac{(4)_\ell}{(7/2)_\ell}, \tag{6.2}$$

with $(p)_\ell = \Gamma(p+\ell)/\Gamma(\ell)$. The higher-order coefficients c_ℓ may be found in Ref. [29]. The on-shell mass $m_{\rm OS}$ appearing in Eq. (6.1) is related to $m_c(\mu)$ as $m_{\rm OS} = m_c(\mu)[1 + \alpha_s/\pi(4/3 - \log m_c(\mu)/\mu)]$ up to $O(\alpha_s^2)$ corrections.

The contribution of this term to the moment $g_{2\ell}^{GG}$ is simply written as

$$g_{2\ell}^{GG} = \frac{\langle(\alpha_s/\pi)G_{\mu\nu}^2\rangle}{(2m_{\rm OS})^4}\left(a_\ell + \frac{\alpha_s}{\pi}c_\ell\right), \tag{6.3}$$

and the reduced moment r_n is modified as

$$r_n^{n-4} = \frac{1}{C_{n/2-1}^{(0)}}\left(C_{n/2-1} + \frac{16\pi^2}{3}\frac{\langle(\alpha_s/\pi)G_{\mu\nu}^2\rangle}{(2m_{\rm OS})^4} \times \left(a_{n/2} + \frac{\alpha_s}{\pi}c_{n/2}\right)\right). \tag{6.4}$$

The numerical coefficients $a_{n/2}$ are 0.179, 0.0, −0.208, −0.449 for $n = 6$, 8, 10, 12, respectively.

The uncertainty for the condensate $\langle(\alpha_s/\pi)G_{\mu\nu}^2\rangle$ is large, i.e., $\langle(\alpha_s/\pi)G_{\mu\nu}^2\rangle = 0.006 \pm 0.012\ \text{GeV}^4$ based on τ decay analysis [30], or from charmonium moments $\langle(\alpha_s/\pi)G_{\mu\nu}^2\rangle = 0.005 \pm 0.004\ \text{GeV}^4$ [31,32], $0.022 \pm 0.004\ \text{GeV}^4$ [33]. In our analysis, we treat $\langle(\alpha_s/\pi)G_{\mu\nu}^2\rangle$ as a free parameter and determine from the charmonium temporal moments together with $m_c(\mu)$ and $\alpha_s(\mu)$. Thus, we avoid further uncertainty from this source.

C. Effect of charm sea quark

Our lattice simulations do not contain a dynamical charm quark, which is expected to be small since the leading contribution from this effect is $O(\alpha_s^2)$ and further suppressed by a factor of $1/m_c^2$. As already discussed, we estimate this contribution from perturbative calculation of $r_n(n_f = 4)/r_n(n_f = 3)$. We correct our lattice calculation $R_n(n_f = 3)$ by multiplying this correction evaluated perturbatively at $O(\alpha_s^3)$ with $m_c(\mu = 3\ \text{GeV}) = 0.9791$ GeV and $\alpha_s(\mu = 3\ \text{GeV}) = 0.2567$, which are taken from the Particle Data Group (PDG). The numerical factor is 1.0031, 1.0014, and 1.0026 for $n = 6$, 8, and 10, respectively, for the pseudoscalar.

VII. DETERMINATION OF $m_c(\mu)$ AND $\alpha_s(\mu)$

We combine the nonperturbative calculation of R_n with the perturbative expansion discussed in the previous sections.

An important issue in the precise determination is that the lattice calculation does not exactly correspond to the experimentally observable η_c and J/ψ mesons. This is because the electromagnetic interaction and the disconnected diagram contributions are missing. Their masses are used to tune the charm quark mass in the lattice calculation, and the mismatch is a potential source of systematic error.

Instead of including the effects of disconnect diagrams and the electromagnetic force in the lattice calculation, we correct the meson masses for these effects. Namely, for the value of $m_{\eta_c}^{\rm exp}$ in Eq. (2.23), we input the experimental value 2,983.6(7) MeV after subtracting the corrections due to disconnected and electromagnetic effects. The effect of disconnected diagrams reduces the η_c mass by 2.4 (8) MeV according to a lattice study [34]. The electromagnetic force is also expected to reduce the η_c mass by 2.6(1.3) MeV [35].

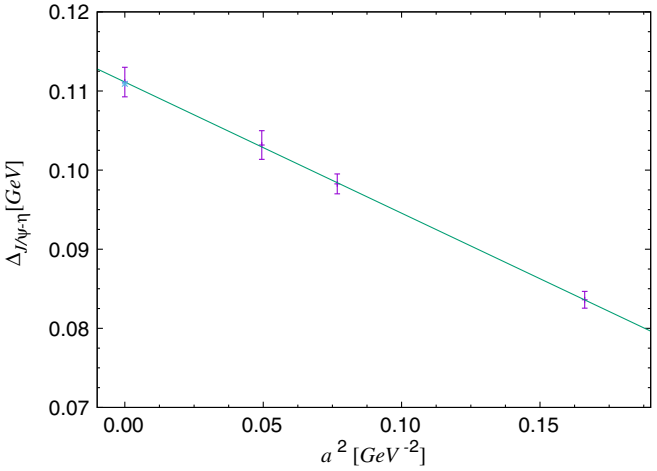

FIG. 7. Hyperfine splitting $\Delta_{J/\psi-\eta_c}$ calculated on the lattice and its continuum extrapolation. The error of lattice scale a from $t^{1/2}$ is added for each data point.

Including these potential systematic effects for the η_c meson mass, we use an input value $m_{\eta_c}^{\rm exp} = 2983.6(0.7) + 2.4(0.8)_{\rm Disc} + 2.6(1.3)_{\rm EM}$ MeV.

The discretization effect may also affect the charmonium mass spectrum calculated on the lattice. The hyperfine splitting $\Delta_{J/\psi-\eta_c} = m_{J/\psi} - m_{\eta_c}$ is known to be sensitive to this source of error. Figure 7 shows $\Delta_{J/\psi-\eta_c}$ as a function of a^2. A significant a^2 dependence is visible on the lattice data especially for the coarsest lattice, for which the value of $\Delta_{J/\psi-\eta_c}$ is about 12% lower than those at two finer lattices. We attempt a continuum extrapolation assuming a linear dependence on a^2. The extrapolation yields 111.4(1.8) MeV, which is consistent with the experimental value, 110.9(2.1) MeV. It provides another evidence that the discretization effect for the charmonium correlator is under good control after the extrapolation by a linear extrapolation in a^2.

Finally, we extract the charm quark mass $m_c(\mu)$, strong coupling constant $\alpha_s(\mu)$, and the gluon condensate $\langle(\alpha/\pi)G^2\rangle/m_{\rm OS}^4$, using Eq. (2.23) with three temporal moments R_6, R_8, and R_{10} as inputs. We also use the ratio of the moments R_6/R_8 as in Eq. (2.24), which is not independent from the individual moments but provides a consistency check as the truncation of perturbative expansion is different.

Figure 8 shows the constraints on $m_c(\mu)$ and $\alpha_s(\mu)$ at $\mu = 3$ GeV given by R_6, R_8, R_{10}, and R_6/R_8. The value of the gluon condensate is tuned such that the combination R_6/R_8, R_8, and R_{10} gives a simultaneous solution. The plot demonstrates that each moment R_n has a sensitivity to a certain combination of $m_c(\mu)$ and $\alpha_s(\mu)$. The ratio R_6/R_8, on the other hand, is sensitive only to $\alpha_s(\mu)$, because by definition (2.24) the ratio depends on $m_c(\mu)$ only logarithmically.

Table IX lists the numerical results for the three parameters including the breakdown of estimated errors. The included errors are from the truncation of the perturbative expansion, statistical uncertainty, the discretization error of $O(a^4)$, finite-volume effects, experimental uncertainty for $m_{\eta_c}^{\rm exp}$, disconnected contributions, and electromagnetic effects. The estimation of these individual errors has already been described in previous sections.

Clearly, the truncation of the perturbative expansion is the dominant source of error for all three of these quantities. As described in the previous section, this source of error is

TABLE IX. Numerical results for $m_c(\mu)$ (top panel), $\alpha_s(\mu)$ (mid panel) and $\frac{\langle(\alpha_s/\pi)G^2\rangle}{m^4}$ (bottom panel). The scale dependent quantities, $m_c(\mu)$ and $\alpha_s(\mu)$, are renormalized at $\mu = 3$ GeV. The results are listed for different choices of three input quantities out of R_6, R_8, R_{10} and R_6/R_8. In addition to the central values with combined errors, the breakdown of the error is presented. They are the estimated errors from the truncation of perturbative expansion, the input value of $t_0^{1/2}$, statistical, discretization error of $O(a^4)$ (or $O(\alpha_s a^2)$), finite volume, experimental data for $m_{\eta_c}^{\rm exp}$, disconnected contribution, electromagnetic effect, in the order given. The total error is estimated by adding the individual errors in quadrature.

Inputs	$m_c(\mu)$ (GeV)	Pert	$t_0^{1/2}$	Stat	$O(a^4)$	Vol	$m_{\eta_c}^{\rm exp}$	Disc	EM
R_6, R_8, R_{10}	1.0032(98)	(82)	(51)	(5)	(16)	(4)	(3)	(4)	(6)
R_6, R_6/R_8, R_{10}	1.0031(194)	(176)	(78)	(6)	(18)	(5)	(4)	(4)	(7)
R_6/R_8, R_8, R_{10}	1.0033(96)	(77)	(49)	(4)	(30)	(4)	(3)	(4)	(6)

Inputs	$\alpha_s(\mu)$	Pert	$t_0^{1/2}$	Stat	$O(a^4)$	Vol	$m_{\eta_c}^{\rm exp}$	Disc	EM
R_6, R_8, R_{10}	0.2530(256)	(213)	(134)	(12)	(38)	(10)	(9)	(10)	(16)
R_6, R_6/R_8, R_{10}	0.2528(127)	(120)	(33)	(2)	(25)	(1)	(0)	(0)	(1)
R_6/R_8, R_8, R_{10}	0.2528(127)	(120)	(32)	(2)	(26)	(1)	(0)	(0)	(1)

Inputs	$\frac{\langle(\alpha_s/\pi)G^2\rangle}{m^4}$	Pert	$t_0^{1/2}$	Stat	$O(a^4)$	Vol	$m_{\eta_c}^{\rm exp}$	Disc	EM
R_6, R_8, R_{10}	−0.0005(99)	(85)	(45)	(4)	(23)	(4)	(3)	(4)	(6)
R_6, R_6/R_8, R_{10}	−0.0006(144)	(133)	(49)	(4)	(23)	(4)	(3)	(3)	(5)
R_6/R_8, R_8, R_{10}	−0.0006(78)	(68)	(29)	(3)	(22)	(3)	(2)	(3)	(5)

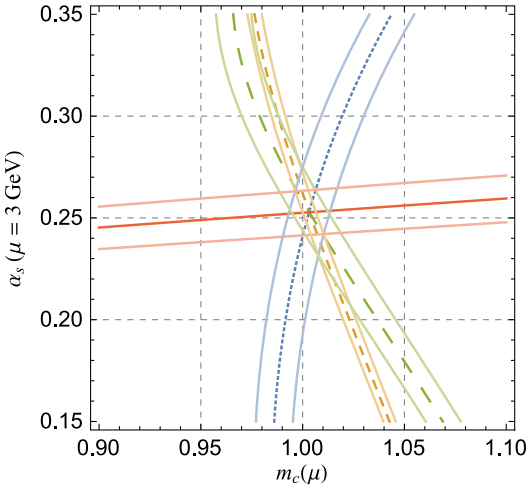

FIG. 8. Constraints on $m_c(\mu)$ and $\alpha_s(\mu)$ from the moments R_6 (dotted curve), R_8 (dashed curve), R_{10} (long dashed curve), and R_6/R_8 (solid curve). For each curve, the band represents the error due to the truncation of perturbative expansion.

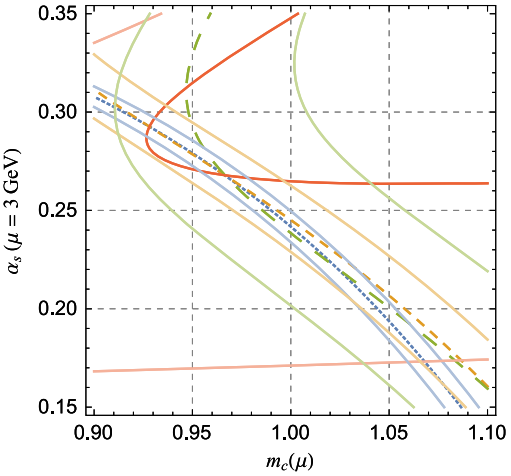

FIG. 9. Constraint from the vector-current moments R_n^V on the $(m_c(\mu), \alpha_s(\mu))$ plane. Dotted, dashed, long-dashed, and solid curves correspond to that of R_6, R_8, R_{10}, and R_6/R_8, respectively.

estimated conservatively by varying the scale μ_m and μ_α in the range between 2 and 4 GeV excluding the region that μ_m/μ_α is far away from 1. The next-largest error comes from the discretization effect estimated by taking two or three data points in the continuum extrapolation. The significance of other sources is not substantial or even negligible when the errors are added in quadrature.

The gluon condensate cannot be determined precisely. In fact, our results are consistent with zero within estimated errors. This is not surprising because this quantity is obtained as a small difference between the perturbative and nonperturbative calculations. It would strongly depend on the order of purturbative expansion. Still, it shows a reasonable agreement with previous phenomenological estimates [30–33].

One may also use the vector channel to extract $m_c(\mu)$ and $\alpha_s(\mu)$ by performing the same analysis. Unfortunately, it was not very successful in our case. As one can see in Fig. 9, the constraints on the $\{m_c(\mu), \alpha_s(\mu)\}$ plane given by different moments R_6, R_8, and R_{10} are similar to each other, and we are not able to disentangle $m_c(\mu)$ and $\alpha_s(\mu)$. (The situation may be different if one can include R_4, but it contains too large a discretization effect, as we discussed.) Therefore, unless we use an input for $\alpha_s(\mu)$ for instance, we are not able to use it to determine $m_c(\mu)$. The statistical error is also three to four times larger for the vector channel.

Therefore, instead of using the vector channel to extract $m_c(\mu)$ and $\alpha_s(\mu)$, we attempt to determine Z_V in Eq. (2.2) with inputs for $m_c(\mu)$ and $\alpha_s(\mu)$ obtained from the pseudoscalar channel. We obtain 0.925(19), 0.937(22), and 0.942(31) for $\beta = 4.17$, 4.35, and 4.47, respectively. These results are to be compared with the determination using the light quark hadron correlators: 0.955(9), 0.964(6), and 0.970(5) [24]. The determination with the charm correlator is slightly lower and has larger errors. The ratio between the two determinations is consistent with 1, after taking the continuum limit.

VIII. CONCLUSION

In this work, we extract the charm quark mass $m_c(\mu)$ and the strong coupling constant $\alpha_s(\mu)$ through the temporal moments of charmonium correlator calculated on lattice ensembles with $2 + 1$ flavors of sea light quarks described by the Möbius domain-wall fermion. The method was originally introduced and developed by the HPQCD and Karlsruhe collaborations [1–3], and we apply it for the lattice data obtained with a different lattice formulation.

The temporal moments in the vector channel can be related to the experimentally available moments of the spectral function and provide the means to validate or to calibrate the lattice calculations. For the determination of $m_c(\mu)$ and $\alpha_s(\mu)$, we use the pseudoscalar channel, since the vector channel does not show enough sensitivity to determine $m_c(\mu)$ and $\alpha_s(\mu)$ separately.

For charm quark, the discretization effect could be sizable. Our lattice simulations are carried out at sufficiently small lattice spacings in the range 0.044–0.080 fm,

TABLE X. Comparison of our results with the values in the Review of Particle Properties [36]. All the quantities are understood to be given in the $\overline{\mathrm{MS}}$ scheme.

	This work	PDG (2014)
$m_c(\mu = 3\ \mathrm{GeV})$	1.0033(96) GeV	
$m_c(\mu = m_c)$	1.2871(123) GeV	1.275(25) GeV
$\alpha_s(\mu = 3\ \mathrm{GeV})$	0.2528(127)	0.2567(34)
$\alpha_s(\mu = M_Z)$	0.1177(26)	0.1185(6)
$\Lambda_{\overline{\mathrm{MS}}}^{n_f=4}$	286(37) MeV	297(8) MeV
$\Lambda_{\overline{\mathrm{MS}}}^{n_f=5}$	205(32) MeV	214(7) MeV

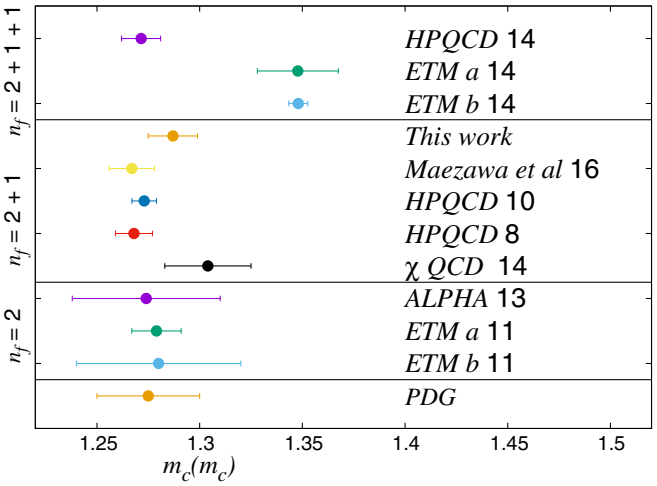

FIG. 10. The charm quark mass obtained in this work is compared with previous lattice determination. The previous results are separately shown for a different number of sea quarks. HPQCD 14 [3], ETM a 14 [37], and ETM b 14 [38] for $n_f = 2+1+1$; Maezawa *et al.* 16 [39], HPQCD 10 [2], HPQCD 08 [1], and χQCD 14 [40] for $n_f = 2+1$; and ALPHA 13 [41], ETM a 11 [42], and ETM b 11 [43] for $n_f = 2$.

and the continuum extrapolation of the temporal moments is under good control.

Our final results are compared with the PDG numbers [36] in Table X, and a comparison with other collaborations is shown in Fig. 10. For our results, we take the values of the smallest total uncertainties from Table IX. The charm quark mass $m_c(\mu = 3\,\mathrm{GeV})$ is converted to $m_c(\mu = m_c)$, and the strong coupling constant $\alpha_s(3\ \mathrm{GeV})$ is converted to the value at the Z boson mass using four-loop running formulas. The threshold effect at the bottom quark mass is incorporated at one loop. The resulting value of $\alpha_s(M_Z)$ is consistent with the PDG.

The result of the HPQCD Collaboration [3] for the charm quark mass is $m_c(3\ \mathrm{GeV}) = 0.9851(63)$ GeV. Our result is $1.8 \pm 1.2\%$ higher. Since the perturbative part of the method is common, a part of the error may be correlated among us.

Among various sources of the systematic error, the dominant one is the truncation of perturbative expansion, which is currently known up to $O(\alpha_s^3)$. To improve the precision on $m_c(\mu)$, therefore, higher-order perturbative calculation has primary importance, as well as the reduction of the scale uncertainty, which is common for all dimensionful parameters.

ACKNOWLEDGMENTS

We thank the members of the JLQCD Collaboration. This work is part of its research programs. Numerical simulations are performed on Hitachi SR16000 and IBM System Blue Gene Solution (Blue Gene/Q) at High Energy Accelerator Research Organization (KEK) under a support of its Large Scale Simulation Program (Grants No. 13/14-04, No. 14/15-10, and No. 15/16-09). This work is supported in part by the Grant-in-Aid of the Japanese Ministry of Education (Grant No. 26247043) and by the Post-K supercomputer project through Joint Institute for Computational Fundamental Science (JICFuS).

APPENDIX: TREE-LEVEL POLE MASS OF DOMAIN-WALL FERMION

At the tree level, the propagator of domain-wall fermion formulation on the lattice is written as [44]

$$\langle q(-p)q(p)\rangle = \frac{-i\gamma_\mu \sin p_\mu + m(1 - W\mathrm{e}^{-\alpha})}{-(1 - W\mathrm{e}^{\alpha}) + m^2(1 - W\mathrm{e}^{-\alpha})}, \quad \text{(A1)}$$

where the Wilson term $W(p)$ is

$$W(p) = 1 - M - r\sum_\mu (1 - \cos p_\mu). \quad \text{(A2)}$$

We take the parameters $M = 1$ and $r = -1$, according to the choice adopted in our simulations.

We obtain the pole mass at the tree level $\tilde{m}_1$ by finding a pole of $\langle q(-p)q(p)\rangle$. For zero spatial momentum, we solve the equation to define the pole with $p_0 = i\tilde{m}_1$. The result is

$$\tilde{m}_1 = \cosh^{-1}\left(\frac{1 - Q + \sqrt{3Q + Q^2}}{2}\right) \quad \text{(A3)}$$

with $Q = ((1 + m^2)/(1 - m^2))^2$.

[1] I. Allison *et al.* (HPQCD Collaboration), Phys. Rev. D **78**, 054513 (2008).
[2] C. McNeile, C. T. H. Davies, E. Follana, K. Hornbostel, and G. P. Lepage, Phys. Rev. D **82**, 034512 (2010).
[3] B. Chakraborty, C. T. H. Davies, B. Galloway, P. Knecht, J. Koponen, G. C. Donald, R. J. Dowdall, G. P. Lepage, and C. McNeile, Phys. Rev. D **91**, 054508 (2015).
[4] R. C. Brower, H. Neff, and K. Orginos, arXiv: 1206.5214.
[5] K. G. Chetyrkin, J. H. Kuhn, and C. Sturm, Eur. Phys. J. C **48**, 107 (2006).

[6] R. Boughezal, M. Czakon, and T. Schutzmeier, Phys. Rev. D **74**, 074006 (2006).
[7] J. H. Kuhn, M. Steinhauser, and C. Sturm, Nucl. Phys. **B778**, 192 (2007).
[8] A. Maier, P. Maierhofer, P. Marquard, and A. V. Smirnov, Nucl. Phys. **B824**, 1 (2010).
[9] A. Maier, P. Maierhofer, and P. Marquard, Nucl. Phys. **B797**, 218 (2008).
[10] A. H. Hoang, V. Mateu, and S. Mohammad Zebarjad, Nucl. Phys. **B813**, 349 (2009).
[11] Y. Kiyo, A. Maier, P. Maierhofer, and P. Marquard, Nucl. Phys. **B823**, 269 (2009).
[12] D. Greynat and S. Peris, Phys. Rev. D **82**, 034030 (2010); **82**, 119907(E) (2010).
[13] D. Greynat, P. Masjuan, and S. Peris, Phys. Rev. D **85**, 054008 (2012).
[14] V. A. Novikov, L. B. Okun, M. A. Shifman, A. I. Vainshtein, M. B. Voloshin, and V. I. Zakharov, Phys. Rep. **41**, 1 (1978).
[15] C. Morningstar and M. J. Peardon, Phys. Rev. D **69**, 054501 (2004).
[16] M. Lüscher, J. High Energy Phys. 08 (2010) 071; 03 (2014) 92.
[17] S. Borsanyi *et al.*, J. High Energy Phys. 09 (2012) 010.
[18] T. Kaneko *et al.* (JLQCD Collaboration), *Proc. Sci.*, LATTICE2013 (2014) 125.
[19] J. Noaki *et al.* (JLQCD Collaboration), *Proc. Sci.*, LATTICE2013 (2014) 263.
[20] H. Fukaya, S. Aoki, G. Cossu, S. Hashimoto, T. Kaneko, and J. Noaki (JLQCD Collaboration), Phys. Rev. D **92**, 111501 (2015).
[21] M. Tomii *et al.* (JLQCD Collaboration), arXiv:1511.09170.
[22] B. Fahy, G. Cossu, S. Hashimoto, T. Kaneko, J. Noaki, and M. Tomii, *Proc. Sci.*, LATTICE2015 (2016) 074.
[23] G. Cossu, J. Noaki, S. Hashimoto, T. Kaneko, H. Fukaya, P. A. Boyle, and J. Doi, arXiv:1311.0084.
[24] M. Tomii *et al.* (JLQCD Collaboration), arXiv:1604.08702.
[25] B. Dehnadi, A. H. Hoang, V. Mateu, and S. M. Zebarjad, J. High Energy Phys. 09 (2013) 103.
[26] J. H. Kuhn and M. Steinhauser, Nucl. Phys. **B619**, 588 (2001); **B640**, 415(E) (2002)].
[27] A. H. Hoang and M. Jamin, Phys. Lett. B **594**, 127 (2004).
[28] B. Dehnadi, A. H. Hoang, and V. Mateu, J. High Energy Phys. 08 (2015) 155.
[29] D. J. Broadhurst, P. A. Baikov, V. A. Ilyin, J. Fleischer, O. V. Tarasov, and V. A. Smirnov, Phys. Lett. B **329**, 103 (1994).
[30] B. V. Geshkenbein, B. L. Ioffe, and K. N. Zyablyuk, Phys. Rev. D **64**, 093009 (2001).
[31] B. L. Ioffe and K. N. Zyablyuk, Eur. Phys. J. C **27**, 229 (2003).
[32] B. L. Ioffe, Prog. Part. Nucl. Phys. **56**, 232 (2006).
[33] S. Narison, Phys. Lett. B **706**, 412 (2012).
[34] E. Follana, Q. Mason, C. Davies, K. Hornbostel, G. P. Lepage, J. Shigemitsu, H. Trottier, and K. Wong (HPQCD and UKQCD Collaborations), Phys. Rev. D **75**, 054502 (2007).
[35] C. T. H. Davies, E. Follana, I. D. Kendall, G. P. Lepage, and C. McNeile (HPQCD Collaboration), Phys. Rev. D **81**, 034506 (2010).
[36] K. A. Olive *et al.* (Particle Data Group Collaboration), Chin. Phys. C **38**, 090001 (2014).
[37] C. Alexandrou, V. Drach, K. Jansen, C. Kallidonis, and G. Koutsou, Phys. Rev. D **90**, 074501 (2014).
[38] N. Carrasco *et al.* (European Twisted Mass Collaboration), Nucl. Phys. **B887**, 19 (2014).
[39] Y. Maezawa and P. Petreczky, arXiv:1606.08798.
[40] Y. B. Yang *et al.*, Phys. Rev. D **92**, 034517 (2015).
[41] J. Heitger, G. M. von Hippel, S. Schaefer, and F. Virotta, *Proc. Sci.*, LATTICE2013 (2014) 475.
[42] K. Jansen, M. Petschlies, and C. Urbach, *Proc. Sci.*, LATTICE2011 (2011) 234.
[43] B. Blossier, P. Dimopoulos, R. Frezzotti, V. Lubicz, M. Petschlies, F. Sanfilippo, S. Simula, and C. Tarantino (ETM Collaboration), Phys. Rev. D **82**, 114513 (2010).
[44] S. Aoki, T. Izubuchi, Y. Kuramashi, and Y. Taniguchi, Phys. Rev. D **67**, 094502 (2003).